Title	Self-supporting carbon nanotube films as flexible neural interfaces
Author(s)	Krukiewicz, Katarzyna; Janas, Dawid; Vallejo-Giraldo, Catalina; Biggs, Manus J. P.
Publication Date	2018-10-26
Publication Information	Krukiewicz, Katarzyna, Janas, Dawid, Vallejo-Giraldo, Catalina, & Biggs, Manus J. P. (2019). Self-supporting carbon nanotube films as flexible neural interfaces. Electrochimica Acta, 295, 253-261. doi: https://doi.org/10.1016/j.electacta.2018.10.157
Publisher	Elsevier
Link to publisher's version	https://doi.org/10.1016/j.electacta.2018.10.157
Item record	http://hdl.handle.net/10379/15024
DOI	http://dx.doi.org/10.1016/j.electacta.2018.10.157

Self-supporting carbon nanotube films as flexible neural interfaces

Katarzyna Krukiewicz[1,2,*], Dawid Janas[2], Catalina Vallejo-Giraldo[1,3], Manus J.P. Biggs[1]

[1]Centre for Research in Medical Devices, National University of Ireland, Galway, Ireland

[2]Department of Chemistry, Silesian University of Technology, Gliwice, Poland

[3]Department of Bioengineering, Imperial College London, London, United Kingdom

*Corresponding author:

Katarzyna Krukiewicz, PhD

Centre for Research in Medical Devices, National University of Ireland, Galway

Newcastle Road, Galway, Ireland

katarzyna.krukiewicz@nuigalway.ie

ISE member

Declarations of interest:

none

Abstract

Advances in neural interface technologies have sought to identify electroactive materials that are able to translate neural depolarisation events into digital signals or modulate neural firing through ionic or electrical stimulation with greater efficiency. An ideal material for neural recording and/or stimulation should possess low electrical impedance coupled with a high cathodic charge storage capacity (CSC_C), charge injection capacity (CIC) and electroactive surface area (ESA), as well as optimal mechanical biomimicry. In this study, we present the robustness of self-supporting CNT films as neural interfaces, combining advantageous electrical and mechanical properties with high cytocompatibility. Films were observed to possess a high CSC_C (29.95 ± 0.91 mC cm^{-2}), CIC (352 ± 5 µC V^{-1} cm^{-2}) and ESA (0.908 ± 0.053 cm^2), low impedance (110 Ω at 1 kHz), low resistance (75 ± 13 Ω) and high capacitance (378 ± 9 µF cm^{-2}), and outperformed Pt control electrodes. Self-supporting CNT films were also found to facilitate neuron growth and decrease the presence of reactive astrocytes in a mixed neural cell population. Self-standing CNT films were shown to be promising materials for the design of flexible and cytocompatible neural interfaces.

Keywords:

CNT; neural interfaces; flexible electronics; neuromodulation; neural recording

1. Introduction

By providing a direct communication route between neural tissue and a man-made digital system, neural interfaces can be used for recording and processing neural activity, or treating neurological disorders [1–3]. Advances in neural interface technologies have sought to identify electroactive materials that are able to translate neural depolarisation events into digital signals or modulate neural firing through ionic or electrical stimulation with greater efficiency [4]. In particular, neuromodulation systems employ stimulating neural electrodes which are implanted into a relevant region of the central or peripheral nervous system. In this way, they are used to deliver a specific prolonged and repetitive electrical signal to target tissues [5]. To provide efficacious and safe stimulation, the electric signal should be sufficient to trigger a physiological response, yet should not damage the peri-electrode tissue nor the electrode itself [6]. Consequently, most applied stimulation protocols employ biphasic current/potential pulses [6,7] with a width in the range from μs to ms [8,9] delivered with a frequencies ranging from 50 Hz to 300 Hz [10,11]. Recent studies, however, suggest that low frequencies can be clinically useful for treating symptoms of Parkinson disease, movement disorders and chronic pain [12–15], and current challenges in the design of neural interfaces are related to the fabrication of materials with optimal electrochemical properties at low frequencies.

Critically, the electrochemical impedance at the tissue-electrode interface should be as low as possible in order to increase the signal to noise ratio and decrease the potentials required to trigger a neuronal response [16]. Charge Storage Capacity (CSC), Charge Injection Capacity (CIC) and Charge Injection Limit (CIL) can be used to assess the amount of charge that can be injected during stimulation [17,18]. Coupled with the Electroactive Surface Area (ESA), a parameter used to describe the actual area of the interface that is able to transmit electric signal [19,20], the consideration of these descriptors are important in neuroelectrode design. Low electrical impedance coupled with high CSC, CIC and ESA represents an ideal material for neural recording and/or stimulation, facilitating low potential stimulation and high sensitivity neural recording.

Following implantation, however, the electrochemical properties of stimulating and recording electrode becomes compromised due to the onset of reactive gliosis, neural encapsulation [21] and chronic BBB disruption [22], a process initiated by mechanical trauma during electrode insertion [23], and exacerbated by chronic relative micromotion at the electrode-tissue interface [24]. Materials commonly used in neuroelectrode fabrication, i.e. crystalline silicon and noble metals, are rigid and exhibit Young's moduli from 70 to 180 GPa, about five orders of magnitude greater than that of i.e. brain tissue (1 kPa) [25]. Current approaches in neural engineering are focused on the design of implantable neural interfaces with optimal mechanical biomimicry, through the development of mechanically soft and flexible neuroelectrode arrays [26–28] which have been shown to reduce reactive gliosis *in vivo* and enhance chronic neuroelectrode functionality [29].

Significant efforts are underway on engineering materials with optimal electrical, biological and mechanical properties for the fabrication of robust electrically stimulating or recording

neural interfaces. Notably, the application of nanotechnology and nanomaterials to design challenges in biomedical engineering have received much attention. Carbon nanotubes (CNT) [30,31], graphene [32,33] and metalic nanowires [34] have been explored as materials for neural tissue engineering, due to their tunable electronic properties, as well as unique mechanical and chemical characteristics [1,35]. In particular, CNTs have been widely studied as electrically active fillers for the fabrication of multifunctional composite materials [36–43]. Conducting CNT nanocomposites have been associated with ongoing limitations, principally related to challenges in the integration of CNTs within the supporting matrix, and in achieving a high CNT concentration. To address these challenges, self-supported, mechanically stable films made entirely of CNT aggregates have been explored as wearable and flexible conductors [44]. Due to their unique fabrication strategy [45] and beneficial electrical properties [44], CNT macroscopic films are promising candidates as neural interfaces. In this study, we present a self-supported, flexible CNT film as a neural interface material, through extensive characterization of the materials electrochemical, mechanical and cytocompatibility properties.

2. Experimental

2.1 Fabrication

Self-supporting CNT films were fabricated from multi-wall CNT arrays formulated by chemical vapour deposition (CVD) of toluene and ferrocene according to procedures reported previously [45–47]. In short, to make a CNT film the material was sonicated (1h, 50% amplitude, Hielscher UP200St 200W sonicator) in iso-propanol in the presence of ethyl cellulose (1:1 weight ratio of polymer to CNTs). A uniform CNT dispersion was then spray-coated onto a Kapton foil, dried, detached from the substrate and annealed in a flame to remove residual ethyl cellulose. The procedure led to the formation of self-standing CNT sheets with the uniform thickness of 10 μm.

2.2 Chemical and morphological characterization

Raman spectra were recorded in the range of 100 cm^{-1} to 3200 cm^{-1} using inVia Renishaw Raman microscope at $\lambda = 514$ nm excitation wavelength. At least 50 accumulations were acquired for each sample for the data to obtain statistical significance. Transmission Electron Microscopy (TEM) images were acquired using FEI Tecnai F20 operating at 60 kV. Scanning Electron Microscopy (SEM) images were collected with a Hitachi S-4700 Scanning Electron Microscope operating at 15 kV.

2.3 Electrochemical characterization

Electrochemical studies were performed by means of a PARSTAT 2273 potentiostat in a three-electrode set-up, comprising a CNT film or Pt foil (0.1 mm thickness, 99.9 % purity, produced by Mennica-Warsaw, Poland) as a working electrode, Ag/AgCl as a reference electrode and glassy carbon rod as an auxiliary electrode. Cyclic voltammograms (CVs) were collected in 0.1 M KCl solution, within the potential range from −0.8 to 1.0 V (*vs.* Ag/AgCl) at 100 mV s^{-1} for 5 CV cycles. CVs were used to compare the electrochemical behaviour of materials and to determine their cathodic Charge Storage Capacity (CSC_C), calculated as the electric charge integrated under corresponding CV curve during the cathodic part of a CV cycle, according to the formula:

$$CSC = \int_{t_1}^{t_2} I(t)dt \quad (1)$$

where t_1 is the beginning of CV cycle, t_2 is the end of CV cycle, and I is the current

Electroactive Surface Area (ESA) measurements were carried out through cyclic voltammetry scans performed in 2.5 μmol cm^{-3} $K_4[Fe(CN)_6]$ 0.1 M KCl solution, in the potential range from −0.2 to 0.6 V (*vs.* Ag/AgCl) at scan rates varied from 0.01 V s^{-1} to 0.2 V s^{-1}. ESA was estimated according to the Randles–Sevcik equation [48,49]:

$$i_p = 2.69 \cdot 10^5 AC\sqrt{Dn^3 v} \quad (2)$$

where i_p is the reduction/oxidation peak current (A), n is the number of electrons contributing to the redox reaction, A is the area of the electrode (cm^2), C is the concentration of $Fe(CN)_6^{4-}$ in the bulk solution (mol cm^{-3}), D is the diffusion coefficient of $Fe(CN)_6^{4-}$ in KCl solution (6.3×10^{-6} cm^2 s^{-1} [50]), and v is the scan rate (V s^{-1}). The measurements were performed in triplicate, the results were expressed as a mean ± standard deviation.

EIS spectra were collected in 0.1 M KCl solution within a frequency range from 100 mHz to 100 kHz, with AC amplitude of 40 mV (*vs.* Ag/AgCl) and DC potential equal to 0 V (*vs.* Ag/AgCl). The results were presented on Bode plots and compared to those of a planar Pt foil electrode. The data fitting analysis was performed using EIS Spectrum Analyzer 1.0 software with the application of the Powell algorithm. In order to assess the goodness of fit, χ^2 were calculated and restricted not to exceed 2 % relative deviation of the calculated spectrum from the measured data.

Capacitances were calculated basing on the parameters of constant phase element (CPE) according to the formula [51]:

$$C = \frac{(Q_0 \cdot R)^{1/n}}{R} \quad (3)$$

where C is the capacitance (F), R is the film resistance (Ω), Q_0 and n are CPE parameters. Charge Injection Capacity (CIC) was studied by integration of chronoamperometric curves used to simulate the parameters of neural stimulation [6–11], i.e. a single biphasic potential pulse consisting of a 5 ms application of a reduction potential followed by a 5 ms application

of an oxidative potential. The potentials were kept in the range from -1.2 V to 1.2 V (*vs*. Ag/AgCl). The experiments were performed in 1x PBS solution.

All electrochemical experiments were performed in triplicates. The results were expressed as the mean of the values ± standard error of the mean.

2.4 Mechanical characterization

To gauge how flexible the CNT films are, a previously reported routine was employed [52]. The specimens (10 mm × 60 mm) were subjected to a three-point bending (Dynamic Mechanical Analysis, TA Instruments Q800DMA) during which electrical resistance was monitored by an on-line source meter (Keithley 2450) connected to a PC. The selected measurement parameters were: 2 bending cycles per minute (1/30 Hz), 1 mm amplitude, 960 cycles (8 h). The variation of electrical resistance as a function of the number of bending cycles gives information about the durability and mechanical integrity of the CNT films when subjected to bending. The measured resistance was normalized to the initial resistance to demonstrate the relative change of the resistance in response to mechanical loading.

2.5 Biological characterization

Primary cultures of a mixed neural population were obtained from the mesencephalon of embryonic Sprague–Dawley rats according to a procedure described previously [53,54]. To visualize neuron and astrocyte cell populations, indirect double-immunofluorescent labelling was applied as described previously [54,55].

An Olympus Fluoview 1000 Confocal Microscope was used to view immunostained samples at a fixed scan size of 1024 × 1024 at a ratio 1:1 and 60× magnification. Cell density was analyzed by counting the number of nuclei corresponding to neurons and astrocytes in an area of 211.97 μm × 211.97 μm in at least 20 random images taken from test and control groups [55]. The quantification of astrocyte area was through ImageJ software (NIH) [56]. The quantification of neurite length was through stereological methods as reported previously [57]. Nine random fields of view from three different technical replicas from five different biological samples were analysed. The average neurite length was calculated according to the formula [58]:

$$L = nT\frac{\pi}{2} \quad (4)$$

where: L is neurite length (μm), n is the number of times neurites intersect with grid lines, T is distance between grid lines (μm).

The biological experiments were conducted to include five biological replicas for both test and control groups. The results were expressed as the mean of the values ± standard error of the mean. A t-test was performed to determine the statistical significance ($p < 0.05$).

3. Results and Discussion

3.1 Chemical and morphological characterization

A fast and convenient method of fabrication led to the formation of robust self-supporting, flexible CNT films with a uniform thickness of 10 µm. SEM micrographs of a CNT film (Fig. 1a) did not reveal the presence of any obvious amounts of contamination in the form of amorphous carbon or residual catalyst. As expected, the films prepared by our method were isotropic with entangled CNTs and their bundles pointing in every direction. Closer investigation by TEM (Fig. 1b) showed that the synthesized CNTs were multi-walled with a diameter of ≅20 nm. The outermost layer of individual CNTs contained some amorphous carbonaceous deposits, but the underlying CNTs were of reasonably high level of graphitization. This had a clear influence on the shape of the collected Raman spectra (Fig. 1c), wherein the I_D/I_G ratio reached 0.50 (the intensity of defect-induced D band to the G mode signalling the graphitic lattice is indicative of the quality of the sample). In our case, the I_D/I_G ratio was elevated by the presence of an extraneous surface coating commonly present on as-made nanocarbon materials [59].

Here Figure 1

3.2 Capacitive behaviour

Neural interfaces can be divided into two group depending on the mechanisms of electron transfer [60]: capacitive materials involve charging and discharging of the electrode-electrolyte double layer, while for other materials, faradaic reactions mediate the flow of electrons. Because faradaic reactions require some species to be oxidized or reduced, which can lead to the degradation of electrode, capacitive materials are more desirable as neural interfaces [60]. To assess whether the material acts through the capacitive or faradaic mechanism, its electrochemical behaviour should be examined e.g. *via* cyclic voltammetry (CV).

CV curves of bare Pt and CNT film presented in Fig. 2a show the lack of a distinctive redox peak system within the potential window from -0.8 V to 1.0 V (*vs*. Ag/AgCl), recognized as the water window for a CNT film [61]. A progressive increase in the anodic current starting from 0.4 V (*vs*. Ag/AgCl), observed in the CV of a CNT film, should be associated with the abundance of defects and amorphous carbonaceous deposits, which is in accordance with the results acquired through Raman spectroscopy and previous literature reports [62]. Both Pt and CNT film can be therefore considered as capacitive materials. For this type of materials, the parameter that is used to quantitatively assess their performance is the cathodic Charge Storage Capacity (CSC_C). Materials possessing high CSC_C, calculated through the integration of CV curve with respect to time (equation 1), are able to store relatively large charges before reaching overpotentials where irreversible faradaic reactions occur [63]. CNTs are well

known for their ability to accumulate charge [64]. This has been verified extensively with CNT/conducting polymer composites, i.e. PEDOT/PSS/MWCNT (CSC_C = 8.6 mC cm^{-2}) [65], in which CNTs were present as a conducting filler component. This charge accumulation was also noted here for self-supporting CNT films, for which the CSC_C (29.95 ± 0.91 mC cm^{-2}) was fourteen times higher relative to bare Pt foil electrodes (2.17 ± 0.10 mC cm^{-2}), indicating their highly capacitive nature. It is worth noting that CNT films can be easily modified to further increase their CSC_C, e.g. through electrochemical deposition of conducting polymers [66].

The increase in CSC_C with respect to Pt is partially related to its elevated Electroactive Surface Area (ESA), describing the total of the surface which is accessible to the electrolyte and can participate in the electron transfer process [19]. Calculated based on the CV curve of a redox probe, $K_4[Fe(CN)_6]$ (Fig.2b), and with the use of Randles-Sevcik equation (equation 2), the ESA of CNT films (0.908 ± 0.053 cm^2) was increased by a factor of 4x relative to Pt control foils (0.238 ± 0.035 cm^2) of the same geometrical dimensions. This maximization of the electrochemically active surface area over a given geometric space resulted in a drastic increase in the capacitance of the material and reduction in electrochemical impedance, which is beneficial for both neural stimulation and recording [67]. By comparing the currents of the anodic and cathodic peaks of a redox probe at different scan rates (Fig.2c), the linear dependency with respect to the square root of scan rate can be observed, indicating a diffusion-limited process with no traces of undesired adsorption of the redox probe onto the surface of CNT film [68,69]. Even when the current density of CV curves is expressed in terms of ESA instead of the geometrical area of the electrodes (Fig.S1), self standing CNT films still outperform bare Pt control, indicating that their ability to accumulate charge is only partially derived from their expanded surface area.

Here Figure 2

3.3 Charge injection capability

In order to negate off-site stimulation or tissue damage, implantable electrodes utilized in neuromodulation and neural stimulation devices should deliver a stable, constant electrical signal for the duration of a stimulating pulse. A cathodal-led, biphasic potential pulse was used to examine the behaviour of the CNT film electrodes relative to control Pt foil electrodes while electrically stimulated (Fig.3a). It was observed that the current recorded with Pt electrodes was not stable, and its magnitude decreased when the potential signal was applied. Following 2.5 ms of applied potential, the current density decreased by 40% relative to that recorded at the onset of stimulation. What is more, a residual current could be noted on the Pt foil electrode after the stimulation pulse was terminated. This kind of electrode instability, derived from the polarization of the electrode, and considered as highly undesirable, has been noted previously for iridium and iridium-oxide alloys electrodes [70].

Conversely, CNT film electrodes demonstrated a current response higher than that of Pt, which was observed to remain constant for the pulse duration. Upon termination of the pulse, the current density abruptly dropped to zero. The integration of current with respect to time gave the Charge Injection Capacity (CIC), which was substantially higher with CNT film electrodes (352 ± 5 μC V^{-1} cm^{-2}) relative to control Pt foil electrodes (138 ± 12 μC V^{-1} cm^{-2}) [71]. It was also observed that the current density and CIC were linearly dependent on the stimulating potential (Fig.3b&c). Since the water window for both electrodes was determined as in the range from -0.8 V to 1 V (*vs.* Ag/AgCl), the maximum CIC that can be applied without triggering water electrolysis [72], namely Charge Injection Limit (CIL), is 352 ± 5 μC cm^{-2} for CNT film and 138 ± 12 μC cm^{-2} for a bare Pt electrode. Critically, neural implants employ charge densities ranging from 2.3 μC cm^{-2} to 2.3 mC cm^{-2} [60], and electrode materials with a high CIC allow for the use of low electrical potentials without compromising the therapeutic effects of stimulation. Indeed, the CIC of 352 ± 5 μC V^{-1} cm^{-2}, as observed with self-supported CNT film electrodes, indicates that therapeutic stimulation could be obtained through a 10 ms potential pulse with a potential of 70 mV [18].

Here Figure 3

3.4 Electrochemical Impedance analysis

Since neuronal signals generally have a very small amplitude, low impedance is a crucial parameter in the development of neural interfaces designed to interface with the central or peripheral nervous system for electrical recording purposes [73]. Although possessing low impedance at high frequencies, metals such as platinum and platinum-iridium exhibit increased impedance at frequencies below 1 kHz. In contrast, the CNT film electrodes demonstrated a stable, low impedance module profile even at low frequencies (> 1 Hz) (Fig.4a), reaching the impedance module of only 430 Ω at 0.1 Hz, almost two orders of magnitude lower than for a Pt control electrode (12 kΩ) at the same frequency. Apart from the low impedance modules, CNT films were also characterized with the low values of the real component of the impedance (Z_{re}), significantly decreased when compared with Pt control electrodes (Fig.S2). Since Z_{re} is directly related to the electrochemical noise of the electrode/electrolyte interface, the decrease in the value of this parameter should result in the more precise collection of neural signals [74].

A substantial shift in the peak frequency in the phase diagram of CNT film (Fig.4b) indicated that the difference in the impedance profile is derived from the capacitive behaviour of this material at frequencies below 10 Hz. Experimental data were subsequently fitted to a simple Randles circuit presented in Fig.4c, which comprised a parallel combination of solution resistance (R_s), charge transfer resistance (R), constant phase element (CPE) and Warburg diffusion element (W_s) [75,76]. The constant phase element replaces typically used double-layer capacitance, showing that the surfaces of both electrodes behave as imperfect capacitors. The constant phase element is in parallel with the resistance R representing the combination

of a charge transfer resistance and polarization resistance, which are the intrinsic properties of the electrode material and can be used to assess its conductivity. Furthermore, low polarization resistance is of a significant importance for the stability of the electrode, which was discussed in the previous section. The simulated data (Tab.S1) confirmed that CNT film electrodes are characterized by low resistance (75 ± 13 Ω) and high capacitance (378 ± 9 μF cm^{-2}), relative to Pt control electrodes (R = 703 ± 151 Ω, C = 18 ± 1 μF cm^{-2}). Interestingly, the electrical resistivity and capacity of experimental CNT film electrodes were superior to materials currently being explored in neural interfaces, such as polypyrrole (R = 6.6 ± 0.1 kΩ, C = 6.6 ± 0.2 μF cm^{-2}) [77] and PEDOT (R = 4.2 ± 0.3 kΩ, C = 13.8 ± 0.1 μF cm^{-2}) [77]. All analysed electrical and electrochemical properties of CNT film and Pt foil electrodes are presented in Table.1.

Here Figure 4 and Table 1

3.5 Mechanical characterization

Self-supporting CNT films have been already explored as wearable and flexible conductors [44]. As shown in [45], various CNT films possess a tensile strength in the range of 85 to 122 MPa, and can be easily bent or strained (Fig.5a) without any loss of performance. To investigate the flexibility of CNT films, the electrical resistance was monitored while films were subjected to repetitive bending (Fig. 5b). After an initial increase of electrical resistance by about 2%, we did not observe any further decrease of conductivity, which remained relatively constant over time. Selected high bend angle may have caused some CNTs and their bundles to lose contact, and so the electrical resistance increased. It is important to note that the bend angles selected for the study represented extreme mechanical conditions.

Here Figure 5

3.6 Biological characterization

To verify the cytocompatibility of experimental CNT film electrodes, primary ventral mesencephalic (VM) mixed cell population was seeded onto the surface of self-supporting CNT films and Pt foil control electrodes, and cultured for 3, 7 and 14 days. At each time point, cells were fixed and processed for immunocytochemical analysis. The cell nuclei (DAPI), neurons (anti-β III tubulin) and astrocytes (anti-GFAP) were stained and cell populations were imaged using scanning confocal microscopy (Fig.6a). Although mixed cell cultures contained oligodendrocytes and microglia populations [78], astrocytes staining was performed in this study to assess the effects of self-supporting CNT films on astrocyte proliferation, neuronal support cells which become activated in response to foreign body

implantation [79,80]. Critically, in a mixed population of neural cells, the ratio between astrocytes and neurons can be used to assess *in vitro* the cytocompatibility of a material in neural systems. The neuron-to-astrocyte ratio (Fig.4b) show the prevalence of neurons after 3 days in culture for both CNT films and Pt control. After 7 days, the ratio of neurons to astrocytes is normalized for Pt but it is increased on self-supporting CNT films. This increased presence of neurons with respect to astrocytes may indicate that this surface promotes neurite viability or adhesion, as described in previous studies [81,82]. Following 14 days of culture, the neuron-to-astrocyte ratio equilibrates for both CNT films and Pt control and equals approximately 1:1.

The differences between CNT film and Pt control materials are observable when the average neurite length of neurons and the mean size of astrocytes are compared. Following 14 days of culture, the average length of neurons when cultured on CNT films was 866 ± 7 μm and only 528 ± 6 μm when cultured on Pt control materials, indicating that self-support CNT films facilitated neurite outgrowth. Furthermore, the mean area of astrocytes soma was significantly lower in cells cultured on self-supporting CNT films (637 ± 54 μm^2) relative to cells cultured on Pt control foils (839 ± 83 μm^2). This difference was significant as an increased cell area is characteristic of astrocyte activation, as seen with reactive gliosis and other neuropathologies [83].

Here Figure 6

4. Conclusions

In this study, the self-supporting CNT films are presented as advantageous materials for the design of neural interfaces. This flexible material made entirely from carbon moieties was found to possess a highly capacitive nature, elevated electrically active surface area and superior charge injection behavior, in theory, allowing for the use of low electrical potentials in neuromodulation approaches without compromising on the therapeutic effects of stimulation. EIS results confirmed that CNT film electrodes are characterized by low resistance and a high capacitance relative to Pt control electrodes and other materials currently being explored as neural interfaces. In contrast to Pt and PtIr electrodes, CNT films demonstrated a stable, low impedance profile at the frequencies below 1 kHz. Cytocompatibility studies indicated the increased presence of neurons with respect to astrocytes, suggesting that CNT film can promote neurite viability or adhesion. Moreover, CNT films were found to facilitate neurite outgrowth, as well as decrease the presence of reactive astrocytes *in vitro,* observed by the decrease in astrocyte cell area. CNT films demonstrated minimal loss of performance following repeated deformation, indicating the potential for this material for the development of flexible neural devices.

Acknowledgements

This publication has emanated from research conducted with the financial support of Science Foundation Ireland (SFI) and is co-funded under the European Regional Development Fund under Grant Number 13/RC/2073 and SFI Technology Innovation Development Programme, grant no. 15/TIDA/2992. This project has received funding from National Science Center, Poland (under the Polonez program, grant agreement UMO-2015/19/P/ST5/03799) and the European Union's Horizon 2020 research and innovation programme under the Marie Skłodowska-Curie grant agreements No. 713690 and 665778. The authors acknowledge the facilities and scientific and technical assistance of the Center for Microscopy & Imaging at the National University of Ireland Galway, a facility that is funded by NUIG and the Irish Government's Programme for Research in Third Level Institutions, Cycles 4 and 5, National Development Plan 2007–2013. D.J. and K.K. would also like to acknowledge the Ministry for Science and Higher Education for the scholarship for outstanding young scientists (0388/E-367/STYP/12/2017 and 649/STYP/12/2017, respectively).

Literature

[1] M. Wang, G. Mi, D. Shi, N. Bassous, D. Hickey, T.J. Webster, Nanotechnology and Nanomaterials for Improving Neural Interfaces, Adv. Funct. Mater. (2018) 1700905. doi:10.1002/adfm.201700905.

[2] W.M. Grill, S.E. Norman, R. V. Bellamkonda, Implanted Neural Interfaces: Biochallenges and Engineered Solutions, Annu. Rev. Biomed. Eng. 11 (2009) 1–24. doi:10.1146/annurev-bioeng-061008-124927.

[3] C. Chiu, X. He, H. Liang, Surface modification of a neural sensor using graphene, Electrochim. Acta. 94 (2013) 42–48. doi:10.1016/j.electacta.2012.12.091.

[4] F.D. Broccard, S. Joshi, J. Wang, G. Cauwenberghs, Neuromorphic neural interfaces: From neurophysiological inspiration to biohybrid coupling with nervous systems, J. Neural Eng. (2017) 041002. doi:10.1088/1741-2552/aa67a9.

[5] M.D. Johnson, H.H. Lim, T.I. Netoff, A.T. Connolly, N. Johnson, A. Roy, A. Holt, K.O. Lim, J.R. Carey, J.L. Vitek, B. He, Neuromodulation for brain disorders: Challenges and opportunities, IEEE Trans. Biomed. Eng. (2013) 610–624. doi:10.1109/TBME.2013.2244890.

[6] D.R. Merrill, M. Bikson, J.G.R. Jefferys, Electrical stimulation of excitable tissue: Design of efficacious and safe protocols, J. Neurosci. Methods. (2005) 171–198. doi:10.1016/j.jneumeth.2004.10.020.

[7] U. Akbar, R.S. Raike, N. Hack, C.W. Hess, J. Skinner, D. Martinez-Ramirez, S. DeJesus, M.S. Okun, Randomized, Blinded Pilot Testing of Nonconventional Stimulation Patterns and Shapes in Parkinson's Disease and Essential Tremor: Evidence for Further Evaluating Narrow and Biphasic Pulses, Neuromodulation. 19 (2016) 343–356. doi:10.1111/ner.12397.

[8] A. Eusebio, W. Thevathasan, L. Doyle Gaynor, A. Pogosyan, E. Bye, T. Foltynie, L. Zrinzo, K. Ashkan, T. Aziz, P. Brown, Deep brain stimulation can suppress pathological synchronisation in parkinsonian patients, J. Neurol. Neurosurg. Psychiatry. 82 (2011) 569–573. doi:10.1136/jnnp.2010.217489.

[9] C.R. Butson, C.C. McIntyre, Tissue and electrode capacitance reduce neural activation volumes during deep brain stimulation, Clin. Neurophysiol. 116 (2005) 16125463. doi:10.1016/j.clinph.2005.06.023.

[10] A.L. Benabid, P. Pollak, D. Gao, D. Hoffmann, P. Limousin, E. Gay, I. Payen, A. Benazzouz, Chronic electrical stimulation of the ventralis intermedius nucleus of the thalamus as a treatment of movement disorders, J. Neurosurg. 84 (1996) 203–214. doi:10.3171/jns.1996.84.2.0203.

[11] C.C. McIntyre, W.M. Grill, Extracellular stimulation of central neurons: influence of stimulus waveform and frequency on neuronal output., J. Neurophysiol. 88 (2002) 1592–1604. doi:DOI 10.1152/jn.00147.2002.

[12] A. Belasen, K. Rizvi, L.E. Gee, P. Yeung, J. Prusik, A. Ramirez-Zamora, E. Hanspal, P. Paiva, J. Durphy, C.E. Argoff, J.G. Pilitsis, Effect of low-frequency deep brain stimulation on sensory thresholds in Parkinson's disease, J. Neurosurg. 126 (2017)

397–403. doi:10.3171/2016.2.JNS152231.

[13] J.F. Baizabal-Carvallo, M. Alonso-Juarez, Low-frequency deep brain stimulation for movement disorders, Parkinsonism Relat. Disord. 31 (2016) 14–22. doi:10.1016/j.parkreldis.2016.07.018.

[14] A. Stefani, A.M. Lozano, A. Peppe, P. Stanzione, S. Galati, D. Tropepi, M. Pierantozzi, L. Brusa, E. Scarnati, P. Mazzone, Bilateral deep brain stimulation of the pedunculopontine and subthalamic nuclei in severe Parkinson's disease, Brain. 130 (2007) 1596–1607. doi:10.1093/brain/awl346.

[15] L. di Biase, A. Fasano, Low-frequency deep brain stimulation for Parkinson's disease: Great expectation or false hope?, Mov. Disord. 31 (2016) 962–967. doi:10.1002/mds.26658.

[16] C. Boehler, T. Stieglitz, M. Asplund, Nanostructured platinum grass enables superior impedance reduction for neural microelectrodes, Biomaterials. 67 (2015) 346–353. doi:10.1016/j.biomaterials.2015.07.036.

[17] E.M. Hudak, D.W. Kumsa, H.B. Martin, J.T. Mortimer, Electron transfer processes occurring on platinum neural stimulating electrodes: Calculated charge-storage capacities are inaccessible during applied stimulation, J. Neural Eng. 14 (2017) 046012. doi:10.1088/1741-2552/aa6945.

[18] D.E. Arreaga-Salas, A. Avendaño-Bolívar, D. Simon, R. Reit, A. Garcia-Sandoval, R.L. Rennaker, W. Voit, Integration of high-charge-injection-capacity electrodes onto polymer softening neural interfaces, ACS Appl. Mater. Interfaces. 7 (2015) 26614–26623. doi:10.1021/acsami.5b08139.

[19] C. Vallejo-Giraldo, K. Krukiewicz, I. Calaresu, J. Zhu, M. Palma, M. Fernandez-Yague, B.W. McDowell, N. Peixoto, N. Farid, G. O'Connor, L. Ballerini, A. Pandit, M.J.P. Biggs, Attenuated Glial Reactivity on Topographically Functionalized Poly(3,4-Ethylenedioxythiophene):P-Toluene Sulfonate (PEDOT:PTS) Neuroelectrodes Fabricated by Microimprint Lithography, Small. 14 (2018) 1800863. doi:10.1002/smll.201800863.

[20] A.R. Harris, P.J. Molino, A.G. Paolini, G.G. Wallace, Effective Area and Charge Density of Chondroitin Sulphate Doped PEDOT Modified Electrodes, Electrochim. Acta. 197 (2016) 99–106. doi:10.1016/j.electacta.2016.03.038.

[21] F. Keohan, X.F. Wei, A. Wongsarnpigoon, E. Lazaro, J.E. Darga, W.M. Grill, Fabrication and evaluation of conductive elastomer electrodes for neural stimulation, J. Biomater. Sci. Polym. Ed. 18 (2007) 1057–1073. doi:10.1163/156856207781494395.

[22] J.P. Seymour, D.R. Kipke, Neural probe design for reduced tissue encapsulation in CNS, Biomaterials. 28 (2007) 3594–3607. doi:10.1016/j.biomaterials.2007.03.024.

[23] J.H. Lee, H. Kim, J.H. Kim, S.H. Lee, Soft implantable microelectrodes for future medicine: Prosthetics, neural signal recording and neuromodulation, Lab Chip. (2016) 959–976. doi:10.1039/c5lc00842e.

[24] H. Lee, R. V. Bellamkonda, W. Sun, M.E. Levenston, Biomechanical analysis of silicon microelectrode-induced strain in the brain, J. Neural Eng. 2 (2005) 81–89. doi:10.1088/1741-2560/2/4/003.

[25] H. Zhang, P.R. Patel, Z. Xie, S.D. Swanson, X. Wang, N.A. Kotov, Tissue-compliant neural implants from microfabricated carbon nanotube multilayer composite, ACS Nano. 7 (2013) 7619–7629. doi:10.1021/nn402074y.

[26] Liang Guo, G.S. Guvanasen, Xi Liu, C. Tuthill, T.R. Nichols, S.P. DeWeerth, A PDMS-based integrated stretchable microelectrode array (isMEA) for neural and muscular surface interfacing., IEEE Trans. Biomed. Circuits Syst. 7 (2013) 1–10. doi:10.1109/TBCAS.2012.2192932.

[27] D. Ziegler, T. Suzuki, S. Takeuchi, Fabrication of flexible neural probes with built-in microfluidic channels by thermal bonding of Parylene, J. Microelectromechanical Syst. 15 (2006) 1477–1482. doi:10.1109/JMEMS.2006.879681.

[28] T. Stieglitz, H. Beutel, M. Schuettler, J.-U. Meyer, Micromachined, Polyimide-Based Devices for Flexible Neural Interfaces, Biomed. Microdevices. 2 (2000) 283–294. doi:10.1023/A:1009955222114.

[29] J.W. Jeong, G. Shin, S. Il Park, K.J. Yu, L. Xu, J.A. Rogers, Soft materials in neuroengineering for hard problems in neuroscience, Neuron. (2015) 175–186. doi:10.1016/j.neuron.2014.12.035.

[30] S. Musa, D.R. Rand, D.J. Cott, J. Loo, C. Bartic, W. Eberle, B. Nuttin, G. Borghs, Bottom-up SiO 2 embedded carbon nanotube electrodes with superior performance for integration in implantable neural microsystems, ACS Nano. 6 (2012) 4615–4628. doi:10.1021/nn201609u.

[31] W. Yi, C. Chen, Z. Feng, Y. Xu, C. Zhou, N. Masurkar, J. Cavanaugh, M. Ming-Cheng Cheng, A flexible and implantable microelectrode arrays using high-temperature grown vertical carbon nanotubes and a biocompatible polymer substrate, Nanotechnology. 26 (2015) 125301. doi:10.1088/0957-4484/26/12/125301.

[32] K. Kostarelos, M. Vincent, C. Hebert, J.A. Garrido, Graphene in the Design and Engineering of Next-Generation Neural Interfaces, Adv. Mater. (2017) 1700909. doi:10.1002/adma.201700909.

[33] N.M. Carretero, M.P. Lichtenstein, E. Pérez, S. Sandoval, G. Tobias, C. Suñol, N. Casan-Pastor, Enhanced charge capacity in iridium oxide-graphene oxide hybrids, Electrochim. Acta. 157 (2015) 369–377. doi:10.1016/j.electacta.2014.10.034.

[34] H.B. Zhou, G. Li, X.N. Sun, Z.H. Zhu, Q.H. Jin, J.L. Zhao, Q.S. Ren, Integration of Au nanorods with flexible thin-film microelectrode arrays for improved neural interfaces, J. Microelectromechanical Syst. 18 (2009) 88–96. doi:10.1109/JMEMS.2008.2011122.

[35] N.A. Kotov, J.O. Winter, I.P. Clements, E. Jan, B.P. Timko, S. Campidelli, S. Pathak, A. Mazzatenta, C.M. Lieber, M. Prato, R. V. Bellamkonda, G.A. Silva, N.W.S. Kam, F. Patolsky, L. Ballerini, Nanomaterials for neural interfaces, Adv. Mater. (2009) 3970–4004. doi:10.1002/adma.200801984.

[36] K. Tegtmeier, P. Aliuos, T. Lenarz, T. Doll, Residual rubber shielded multi walled carbon nanotube electrodes for neural interfacing in active medical implants, Phys. Med. 1 (2016) 8–19. doi:10.1016/j.phmed.2016.04.001.

[37] J. Zhang, X. Liu, W. Xu, W. Luo, M. Li, F. Chu, L. Xu, A. Cao, J. Guan, S. Tang, X. Duan, Stretchable Transparent Electrode Arrays for Simultaneous Electrical and

Optical Interrogation of Neural Circuits in Vivo, Nano Lett. 18 (2018) 2903–2911. doi:10.1021/acs.nanolett.8b00087.

[38] X. Shi, Y. Xiao, H. Xiao, G. Harris, T. Wang, J. Che, Topographic guidance based on microgrooved electroactive composite films for neural interface, Colloids Surfaces B Biointerfaces. 145 (2016) 768–776. doi:10.1016/j.colsurfb.2016.05.086.

[39] S. Carli, L. Lambertini, E. Zucchini, F. Ciarpella, A. Scarpellini, M. Prato, E. Castagnola, L. Fadiga, D. Ricci, Single walled carbon nanohorns composite for neural sensing and stimulation, Sensors Actuators, B Chem. 271 (2018) 280–288. doi:10.1016/j.snb.2018.05.083.

[40] S. Chen, W. Pei, Q. Gui, R. Tang, Y. Chen, S. Zhao, H. Wang, H. Chen, PEDOT/MWCNT composite film coated microelectrode arrays for neural interface improvement, Sensors Actuators, A Phys. 193 (2013) 141–148. doi:10.1016/j.sna.2013.01.033.

[41] V. Kuzmenko, E. Karabulut, E. Pernevik, P. Enoksson, P. Gatenholm, Tailor-made conductive inks from cellulose nanofibrils for 3D printing of neural guidelines, Carbohydr. Polym. 189 (2018) 22–30. doi:10.1016/j.carbpol.2018.01.097.

[42] N. Singh, J. Chen, K.K. Koziol, K.R. Hallam, D. Janas, A.J. Patil, A. Strachan, J.G. Hanley, S.S. Rahatekar, Chitin and carbon nanotube composites as biocompatible scaffolds for neuron growth, Nanoscale. 8 (2016) 8288–8299. doi:10.1039/c5nr06595j.

[43] F. Pouladzadeh, A.A. Katbab, N. Haghighipour, E. Kashi, Carbon nanotube loaded electrospun scaffolds based on thermoplastic urethane (TPU) with enhanced proliferation and neural differentiation of rat mesenchymal stem cells: The role of state of electrical conductivity, Eur. Polym. J. 105 (2018) 286–296. doi:https://doi.org/10.1016/j.eurpolymj.2018.05.011.

[44] D. Janas, Powerful doping of chirality-sorted carbon nanotube films, Vacuum. 149 (2018) 48–52. doi:10.1016/j.vacuum.2017.12.013.

[45] D. Janas, M. Rdest, K.K.K. Koziol, Free-standing films from chirality-controlled carbon nanotubes, Mater. Des. 121 (2017) 119–125. doi:10.1016/j.matdes.2017.02.062.

[46] C. Singh, M.S.P. Shaffer, A.H. Windle, Production of controlled architectures of aligned carbon nanotubes by an injection chemical vapour deposition method, Carbon N. Y. 41 (2003) 359–368. doi:10.1016/S0008-6223(02)00314-7.

[47] D. Janas, G. Stando, Unexpectedly strong hydrophilic character of free-standing thin films from carbon nanotubes, Sci. Rep. 7 (2017) 12274. doi:10.1038/s41598-017-12443-y.

[48] A.J. Bard, L.R. Faulkner, Electrochemical Methods: Fundamentals and Applications, 2001. doi:10.1016/B978-0-12-381373-2.00056-9.

[49] M. Libansky, J. Zima, J. Barek, A. Reznickova, V. Svorcik, H. Dejmkova, Basic electrochemical properties of sputtered gold film electrodes, Electrochim. Acta. 251 (2017) 452–460. doi:10.1016/j.electacta.2017.08.048.

[50] N.P.C. Stevens, M.B. Rooney, A.M. Bond, S.W. Feldberg, A Comparison of Simulated and Experimental Voltammograms Obtained for the [Fe(CN) 6] 3-/4- Couple in the

Absence of Added Supporting Electrolyte at a Rotating Disk Electrode, J. Phys. Chem. A. 105 (2001) 9085–9093. doi:10.1021/jp0103878.

[51] X. Yuan, Z.F. Yue, X. Chen, S.F. Wen, L. Li, T. Feng, EIS study of effective capacitance and water uptake behaviors of silicone-epoxy hybrid coatings on mild steel, Prog. Org. Coatings. 51 (2015) 2821–2829. doi:10.1016/j.porgcoat.2015.04.004.

[52] D. Janas, S.K. Kreft, K.K.K. Koziol, Printing of highly conductive carbon nanotubes fibres from aqueous dispersion, Mater. Des. 116 (2017) 16–20. doi:10.1016/j.matdes.2016.11.073.

[53] C. Vallejo-Giraldo, N.P. Pampaloni, A.R. Pallipurath, P. Mokarian-Tabari, J. O'Connell, J.D. Holmes, A. Trotier, K. Krukiewicz, G. Orpella-Aceret, E. Pugliese, L. Ballerini, M. Kilcoyne, E. Dowd, L.R. Quinlan, A. Pandit, P. Kavanagh, M.J.P. Biggs, Preparation of Cytocompatible ITO Neuroelectrodes with Enhanced Electrochemical Characteristics Using a Facile Anodic Oxidation Process, Adv. Funct. Mater. 28 (2017) 1605035. doi:10.1002/adfm.201605035.

[54] K. Krukiewicz, M. Chudy, C. Vallejo-Giraldo, M. Skorupa, D. Więcławska, R. Turczyn, M. Biggs, Fractal form PEDOT/Au assemblies as thin-film neural interface materials, Biomed. Mater. 13 (2018) 54102. http://stacks.iop.org/1748-605X/13/i=5/a=054102.

[55] C. Vallejo-Giraldo, E. Pugliese, A. Larrañaga, M.A. Fernandez-Yague, J.J. Britton, A. Trotier, G. Tadayyon, A. Kelly, I. Rago, J.R. Sarasua, E. Dowd, L.R. Quinlan, A. Pandit, M.J.P. Biggs, Polyhydroxyalkanoate/carbon nanotube nanocomposites: Flexible electrically conducting elastomers for neural applications, Nanomedicine. 11 (2016) 2547–2563. doi:10.2217/nnm-2016-0075.

[56] J. Lobo, E.Y.S. See, M. Biggs, A. Pandit, An insight into morphometric descriptors of cell shape that pertain to regenerative medicine, J. Tissue Eng. Regen. Med. (2016) 539–553. doi:10.1002/term.1994.

[57] G.W. O'Keeffe, P. Dockery, A.M. Sullivan, Effects of growth/differentiation factor 5 on the survival and morphology of embryonic rat midbrain dopaminergic neurones in vitro, J. Neurocytol. 33 (2004) 479–488. doi:10.1007/s11068-004-0511-y.

[58] E.T. Kavanagh, J.P. Loughlin, K.R. Herbert, P. Dockery, A. Samali, K.M. Doyle, A.M. Gorman, Functionality of NGF-protected PC12 cells following exposure to 6-hydroxydopamine, Biochem. Biophys. Res. Commun. 351 (2006) 890–895. doi:10.1016/j.bbrc.2006.10.104.

[59] S. Boncel, R.M. Sundaram, A.H. Windle, K.K.K. Koziol, Enhancement of the mechanical properties of directly spun CNT fibers by chemical treatment, ACS Nano. 5 (2011) 9339–9344. doi:10.1021/nn202685x.

[60] S.F. Cogan, Neural Stimulation and Recording Electrodes, Annu. Rev. Biomed. Eng. 10 (2008) 275–309. doi:10.1146/annurev.bioeng.10.061807.160518.

[61] S. Negi, R. Bhandari, L. Rieth, R. Van Wagenen, F. Solzbacher, Neural electrode degradation from continuous electrical stimulation: Comparison of sputtered and activated iridium oxide, J. Neurosci. Methods. 186 (2010) 8. doi:10.1016/j.jneumeth.2009.10.016.

[62] K. Krukiewicz, M. Krzywiecki, M.J.P. Biggs, D. Janas, Chirality-sorted carbon nanotube films as high capacity electrode materials, RSC Adv. 8 (2018) 30600–30609. doi:10.1039/C8RA03963A.

[63] J. Arle, J. Shils, Essential Neuromodulation, 2011. doi:10.1016/C2009-0-61346-5.

[64] T. Chen, L. Dai, Carbon nanomaterials for high-performance supercapacitors, Mater. Today. 16 (2013) 272–280. doi:10.1016/j.mattod.2013.07.002.

[65] K. Wang, R.Y. Tang, X.B. Zhao, J.J. Li, Y.R. Lang, X.X. Jiang, H.J. Sun, Q.X. Lin, C.Y. Wang, Covalent bonding of YIGSR and RGD to PEDOT/PSS/MWCNT-COOH composite material to improve the neural interface, Nanoscale. 7 (2015) 18677–18685. doi:10.1039/c5nr05784a.

[66] K. Krukiewicz, J.S. Bulmer, D. Janas, K.K.K. Koziol, J.K. Zak, Poly(3,4-ethylenedioxythiophene) growth on the surface of horizontally aligned MWCNT electrode, Appl. Surf. Sci. 335 (2015) 130–136. http://www.sciencedirect.com/science/article/pii/S0169433215003347.

[67] K.A. Ludwig, J.D. Uram, J. Yang, D.C. Martin, D.R. Kipke, Chronic neural recordings using silicon microelectrode arrays electrochemically deposited with a poly(3,4-ethylenedioxythiophene) (PEDOT) film, J. Neural Eng. 3 (2006) 59–70. doi:10.1088/1741-2560/3/1/007.

[68] H.I. Karunadasa, E. Montalvo, Y. Sun, M. Majda, J.R. Long, C.J. Chang, A molecular MoS2 edge site mimic for catalytic hydrogen generation, Science (80-.). 335 (2012) 698–702. doi:10.1126/science.1215868.

[69] N. Elgrishi, K.J. Rountree, B.D. McCarthy, E.S. Rountree, T.T. Eisenhart, J.L. Dempsey, A Practical Beginner's Guide to Cyclic Voltammetry, J. Chem. Educ. 95 (2018) 197–206. doi:10.1021/acs.jchemed.7b00361.

[70] S. Wilks, S. Richardson-Burns, J. Hendricks, D.C. Martin, K. Otto, Poly(3,4-ethylene dioxythiophene) (PEDOT) as a micro-neural interface material for electrostimulation, Front. Neuroeng. (2009). doi:10.3389/neuro.16.007.2009.

[71] R.T. Leung, M.N. Shivdasani, D.A.X. Nayagam, R.K. Shepherd, In vivo and in vitro comparison of the charge injection capacity of platinum macroelectrodes, IEEE Trans. Biomed. Eng. 62 (2015) 849–857. doi:10.1109/TBME.2014.2366514.

[72] T.L. Rose, L.S. Robblee, Electrical Stimulation with Pt Electrodes. VIII. Electrochemically Safe Charge Injection Limits with 0.2 MS Pulses, IEEE Trans. Biomed. Eng. 37 (1990) 1118–1120. doi:10.1109/10.61038.

[73] S.J. Paik, Y. Park, D.I.D. Cho, Roughened polysilicon for low impedance microelectrodes in neural probes, J. Micromechanics Microengineering. 13 (2003) 373–379. doi:10.1088/0960-1317/13/3/304.

[74] P.R.F. Rocha, P. Schlett, U. Kintzel, V. Mailänder, L.K.J. Vandamme, G. Zeck, H.L. Gomes, F. Biscarini, D.M. De Leeuw, Electrochemical noise and impedance of Au electrode/electrolyte interfaces enabling extracellular detection of glioma cell populations, Sci. Rep. 6 (2016) 34843. doi:10.1038/srep34843.

[75] P. A. Basnayaka, M. K. Ram, L. Stefanakos, A. Kumar, Graphene/Polypyrrole

Nanocomposite as Electrochemical Supercapacitor Electrode: Electrochemical Impedance Studies, Graphene. 2 (2013) 81–87. doi:10.4236/graphene.2013.22012.

[76] Y. Braham, H. Barhoumi, A. Maaref, A. Bakhrouf, C.G. Heywang, T.C. Bouhacina, N. Jaffrezic-Renault, Characterization of Urea Biosensor Based on the Immobilization of Bacteria Proteus Mirabilis in Interaction with Iron Oxide Nanoparticles on Gold Electrode, J. Biosens. Bioelectron. 6 (2015) 100016. doi: 10.4172/2155-6210.1000160.

[77] M.R. Abidian, D.C. Martin, Experimental and theoretical characterization of implantable neural microelectrodes modified with conducting polymer nanotubes, Biomaterials. 29 (2008) 1273–1283. doi:10.1016/j.biomaterials.2007.11.022.

[78] S.H. Chen, E.A. Oyarzabal, J.S. Hong, Preparation of rodent primary cultures for neuron-glia, mixed glia, enriched microglia, and reconstituted cultures with microglia, Methods Mol. Biol. 1041 (2013) 231–240. doi:10.1007/978-1-62703-520-0_21.

[79] P. Pierozan, F. Ferreira, B.O. de Lima, R. Pessoa-Pureur, Quinolinic acid induces disrupts cytoskeletal homeostasis in striatal neurons. Protective role of astrocyte-neuron interaction, J. Neurosci. Res. 93 (2015) 268–284. doi:10.1002/jnr.23494.

[80] A. Goudriaan, N. Camargo, K.E. Carney, S.H.R. Oliet, A.B. Smit, M.H.G. Verheijen, Novel cell separation method for molecular analysis of neuron-astrocyte co-cultures, Front. Cell. Neurosci. 8 (2014) 12. doi:10.3389/fncel.2014.00012.

[81] T. Gabay, E. Jakobs, E. Ben-Jacob, Y. Hanein, Engineered self-organization of neural networks using carbon nanotube clusters, Phys. A Stat. Mech. Its Appl. 350 (2005) 611–621. doi:10.1016/j.physa.2004.11.007.

[82] P. Roach, T. Parker, N. Gadegaard, M.R. Alexander, Surface strategies for control of neuronal cell adhesion: A review, Surf. Sci. Rep. 65 (2010) 145–173. doi:10.1016/j.surfrep.2010.07.001.

[83] U. Wilhelmsson, E.A. Bushong, D.L. Price, B.L. Smarr, V. Phung, M. Terada, M.H. Ellisman, M. Pekny, Redefining the concept of reactive astrocytes as cells that remain within their unique domains upon reaction to injury, Proc. Natl. Acad. Sci. 103 (2006) 17513–17518. doi:10.1073/pnas.0602841103.

Figures & captions

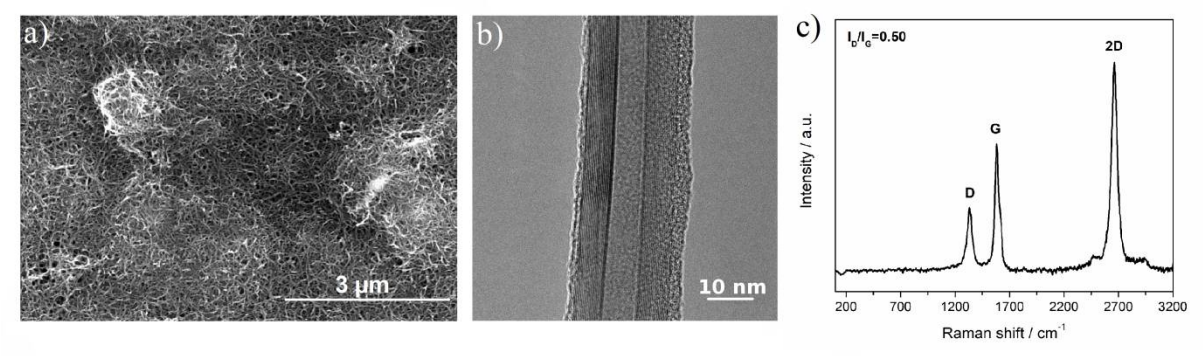

Fig.1. Characterization of CNT films: SEM micrograph (a); TEM micrograph (b); Raman spectrum (c).

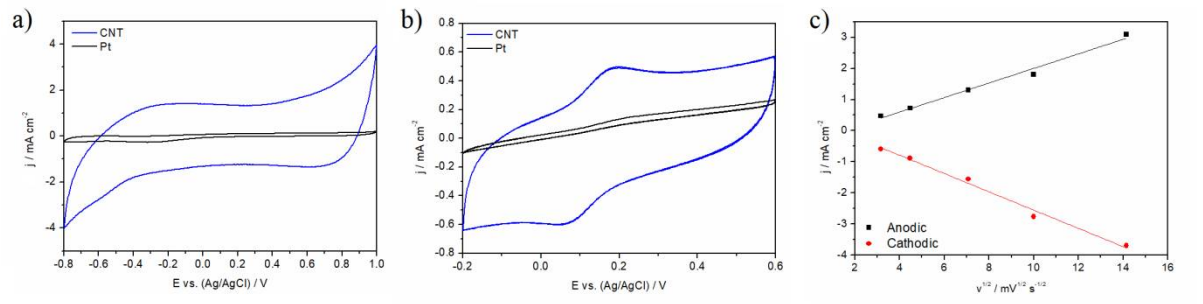

Fig.2. Cyclic voltammograms collected in 0.1 M KCl at a scan rate of 0.1 V s^{-1} on CNT film electrode (blue line) and Pt foil control electrodes (black line) (a); cyclic voltammograms collected in the presence of a redox probe, $K_4[Fe(CN)_6]$, in 0.1 M KCl at a scan rate of 0.01 V s^{-1} of CNT film electrode (blue line) and Pt foil control electrode (black line) (b); current densities at a cathodic (red dots) and anodic (black squares) peak of $K_4[Fe(CN)_6]$ redox system collected on CNT film working electrodes as a function of the square root of the scan rate (c).

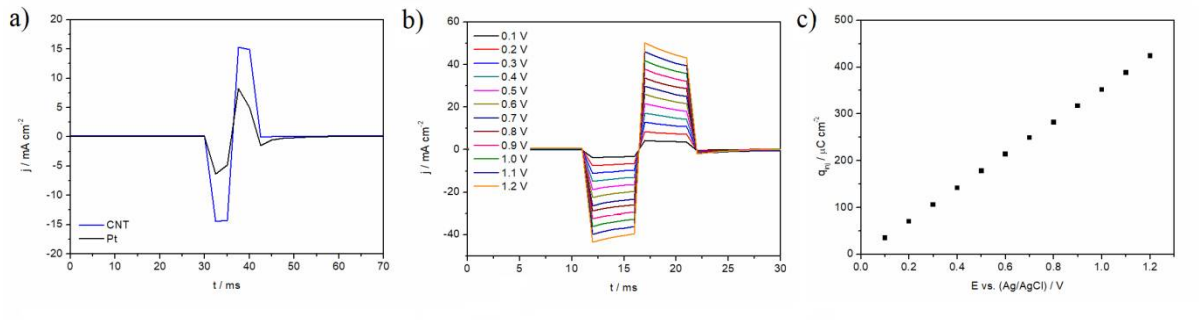

Fig.3. A cathodal-led, biphasic potential pulse of ±0.5 V *vs.* Ag/AgCl (10 ms) collected on CNT film electrodes (blue line) and Pt foil control electrodes (black line) in 1 x PBS solution (a); Stimulation pulse (b) and injected current (q_{inj}, CIC) (c) collected on CNT film electrodes in 1 x PBS solution as a function of a stimulation potential.

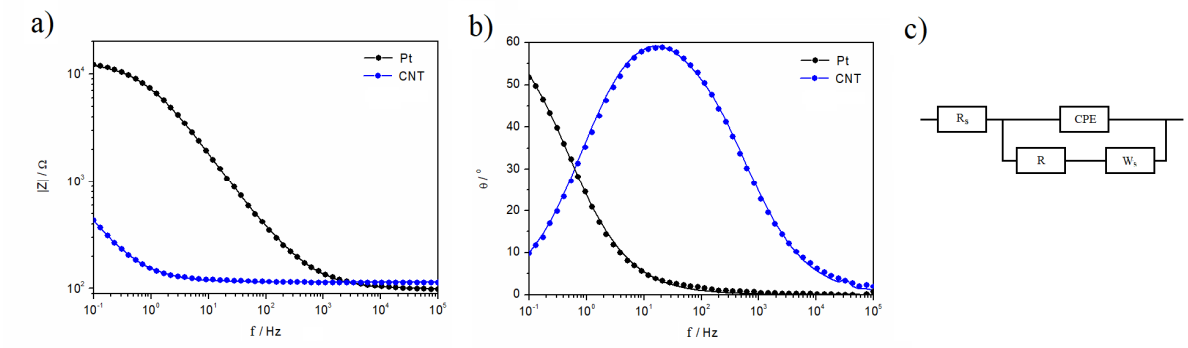

Fig.4. Bode plots comparing EIS spectra of CNT film and Pt control electrodes in the form of impedance modulus *vs.* frequency (a) and phase *vs.* frequency (b), as well as the equivalent circuit used for fitting (c); dots represent experimental data, while lines represent simulated results. EIS spectra were collected in 0.1 M KCl solution with AC amplitude of 40 mV (*vs.* Ag/AgCl) and DC potential equal to 0 V (*vs.* Ag/AgCl).

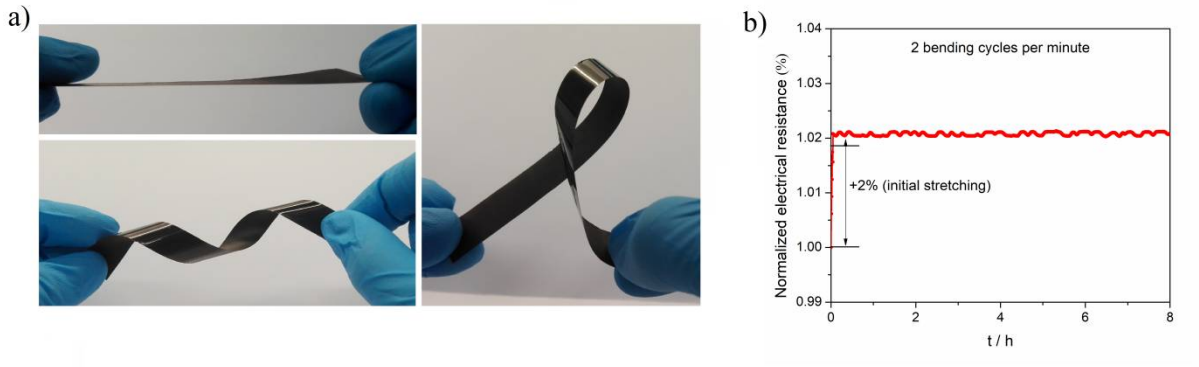

Fig.5. The behaviour of CNT films during bending (a); stability of electrical resistance of the CNT film subjected to repeated bending (b).

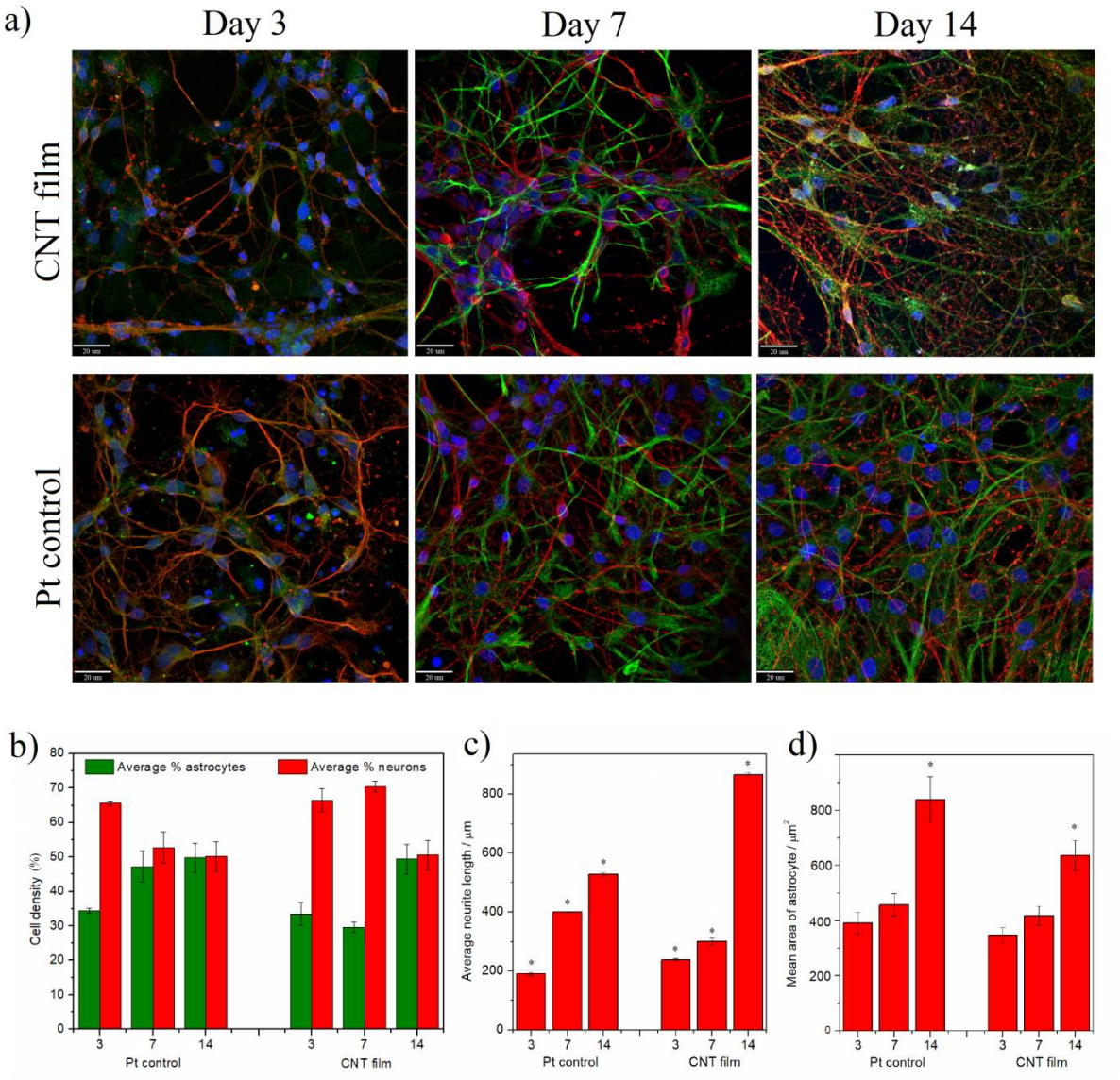

Fig.6. Fluorescent images of primary ventral mesencephalic (VM) mixed cell population grown on CNT films and Pt control substrates for 3, 7 and 14 days; neurons are visualized by anti-β III tubulin (red), astrocyte cells by anti-GFAP (green) and nuclei by DAPI (blue), scale bar = 20 µm (a); cell density (%) of astrocytes and neurons on CNT films and Pt control substrates (b); average neurite length, µm (c); mean area of astrocytes, μm^2 (d); results are ± STD, ★ = $p < 0.05$, N=5.

Tables

Tab.1. Electrochemical properties of CNT film and Pt control electrodes, including cathodal Charge Storage Capacity (CSC_C), Electroactive Surface Area (ESA), Charge Injection Capacity (CIC), Resistance (R) and Capacitance (C); results are expressed as the mean of the values ± standard deviation.

	Pt control	**CNT film**
CSC_C / mC cm^{-2}	2.17 ± 0.10	29.95 ± 0.91
ESA / cm^2	0.238 ± 0.035	0.908 ± 0.053
CIC / µC V^{-1} cm^{-2}	138 ± 12	352 ± 5
R / Ω	703 ± 151	75 ± 13
C / µF cm^{-2}	18 ± 1	378 ± 9